Report

Current Biology

# Genomic targets of hurricane-induced selection on clinging performance in an island lizard

## Highlights

- Hurricane survivors show parallel selection at musculoskeletal loci
- *hs6st1* is the top candidate for rear toe length genome wide
- CRISPR *hs6st1* knockout reduces anole hindfoot skeletal elements
- Shorter rear toe elements improve clinging during simulated storms

## Authors

Princeton L. Vaughn, Colin M. Donihue, Andrea D. Rummel, ..., Jason Kolbe, Jonathan Losos, Shane C. Campbell-Staton

## Correspondence

scampbellstaton@princeton.edu

## In brief

Vaughn et al. show that hurricanes drive parallel genomic selection signatures in island anoles. One candidate locus (*hs6st1*) is associated with rear toe length. CRISPR disruption reduces hindfoot elements, and shorter rear toes improve clinging ability in high winds, linking extreme-weather selection to morphology, performance, and development in the wild.

Vaughn et al., 2026, Current Biology *36*, 1–9
August 17, 2026 
https://doi.org/10.1016/j.cub.2026.07.022

CellPress

Please cite this article in press as: Vaughn et al., Genomic targets of hurricane-induced selection on clinging performance in an island lizard, Current Biology (2026), https://doi.org/10.1016/j.cub.2026.07.022

Current Biology

CellPress
OPEN ACCESS

Report

# Genomic targets of hurricane-induced selection on clinging performance in an island lizard

Princeton L. Vaughn,[1] Colin M. Donihue,[2,3] Andrea D. Rummel,[1,4] Nicolas C. Rochette,[1] Douglas B. Menke,[5] Amber L. Rittgers,[5] Christina E. Sabin,[5,6] Anna L. Iouchmanov,[5] Aaron H. Griffing,[7,8,9] Anthony Herrel,[10,11,12,13] Jason Kolbe,[14] Jonathan Losos,[2] and Shane C. Campbell-Staton[1,15,*]

[1]Department of Ecology and Evolutionary Biology, Princeton University, Princeton, NJ 08544, USA
[2]Department of Biology, Washington University in St. Louis, St. Louis, MO 63130, USA
[3]Institute at Brown for Environment and Society, Brown University, Providence, RI 02912, USA
[4]Department of Biosciences, Rice University, Houston, TX 77005, USA
[5]Department of Genetics, University of Georgia, Athens, GA 30602, USA
[6]Department of Cellular Biology, University of Georgia, Athens, GA 30602, USA
[7]Department of Molecular Biology, Princeton University, Princeton, NJ 08544, USA
[8]Department of Chemical & Biological Engineering, Princeton University, Princeton, NJ 08544, USA
[9]Department of Geosciences, Princeton University, Princeton, NJ 08544, USA
[10]Mécanismes Adaptatifs et Evolution, UMR 7179, Muséum national d'Histoire naturelle CNRS, 75005 Paris, France
[11]Department of Biology, Evolutionary Morphology of Vertebrates, Ghent University, 9000 Ghent, Belgium
[12]Functional Morphology Laboratory, Department of Biology, University of Antwerp, 2000 Antwerp, Belgium
[13]Naturhistorisches Museum Bern, 3005 Bern, Switzerland
[14]Department of Biological Sciences, University of Rhode Island, Kingston, RI 02881, USA
[15]Lead contact
*Correspondence: scampbellstaton@princeton.edu
https://doi.org/10.1016/j.cub.2026.07.022

## SUMMARY

A central goal of evolutionary biology is to understand the molecular mechanisms that enable adaptive responses to novel environmental pressures. Extreme weather events like natural disasters can have catastrophic impacts on wildlife via habitat destruction, mortality,[1–6] population displacement,[6,7] and natural selection,[1,2,5,8,9] even shaping broad biogeographic patterns of local adaptation on phylogenetic scales.[10,11] However, few studies have investigated the functional changes in organismal performance or genomic targets associated with responses to such events.[2,12–14] Here, we investigate mechanisms of hurricane-mediated selection associated with parallel morphological shifts observed in a small island endemic lizard, the Silver Key Anole (*Anolis scriptus*), on two islands of the Turks and Caicos struck by hurricanes Irma and Maria in 2017.[9] These observed changes suggest directional selection on clinging ability in the face of hurricane-force winds.[9,10,12,15] Genome scans for parallel selection identified five loci with known roles in musculoskeletal development and function. Among these loci, *hs6st1* displayed the most significant genome-wide association with the length of the longest rear toe. CRISPR-induced knockout of *hs6st1* resulted in significant toe length reduction and complete toe agenesis. Simulated high wind speeds revealed that shorter rear toe length was associated with greater clinging performance in anoles. This study highlights the interactions between performance, morphology, and genetic variation underlying rapid adaptive responses to extreme weather events in the wild. As extreme weather events become more frequent and severe in the coming decades,[16,17] understanding their evolutionary impacts will be critical for assessing their long-term effects on the world's biodiversity.[18]

## RESULTS AND DISCUSSION

### Parallel hurricane-induced selection on musculoskeletal development loci

Genome-wide reduced representation sequencing (RAD-seq[19,20]) of tissue samples collected from lizards on Pine Cay and Water Cay before (2017; Pine Cay: $n$ = 20; Water Cay: $n$ = 20) and after (2018; Pine Cay: $n$ = 61; Water Cay: $n$ = 62; Figure 1A) hurricanes Irma and Maria revealed no evidence of storm-mediated interisland dispersal. Principal components analysis of 221,549 genome-wide single-nucleotide polymorphisms (SNPs) revealed significant genetic differentiation between island populations but no detectable differentiation between pre- and post-hurricane samples on either island (Figure 1B). Discriminant function analysis identified two population clusters (k = 2, BIC = 1,210.424; Figure S1A) as the best-fit model for the data, aligning perfectly with island of origin (membership probability = 100; Figure 1B). These results support independent and parallel selection of morphology across genetically distinct island populations.

Please cite this article in press as: Vaughn et al., Genomic targets of hurricane-induced selection on clinging performance in an island lizard, Current Biology (2026), https://doi.org/10.1016/j.cub.2026.07.022



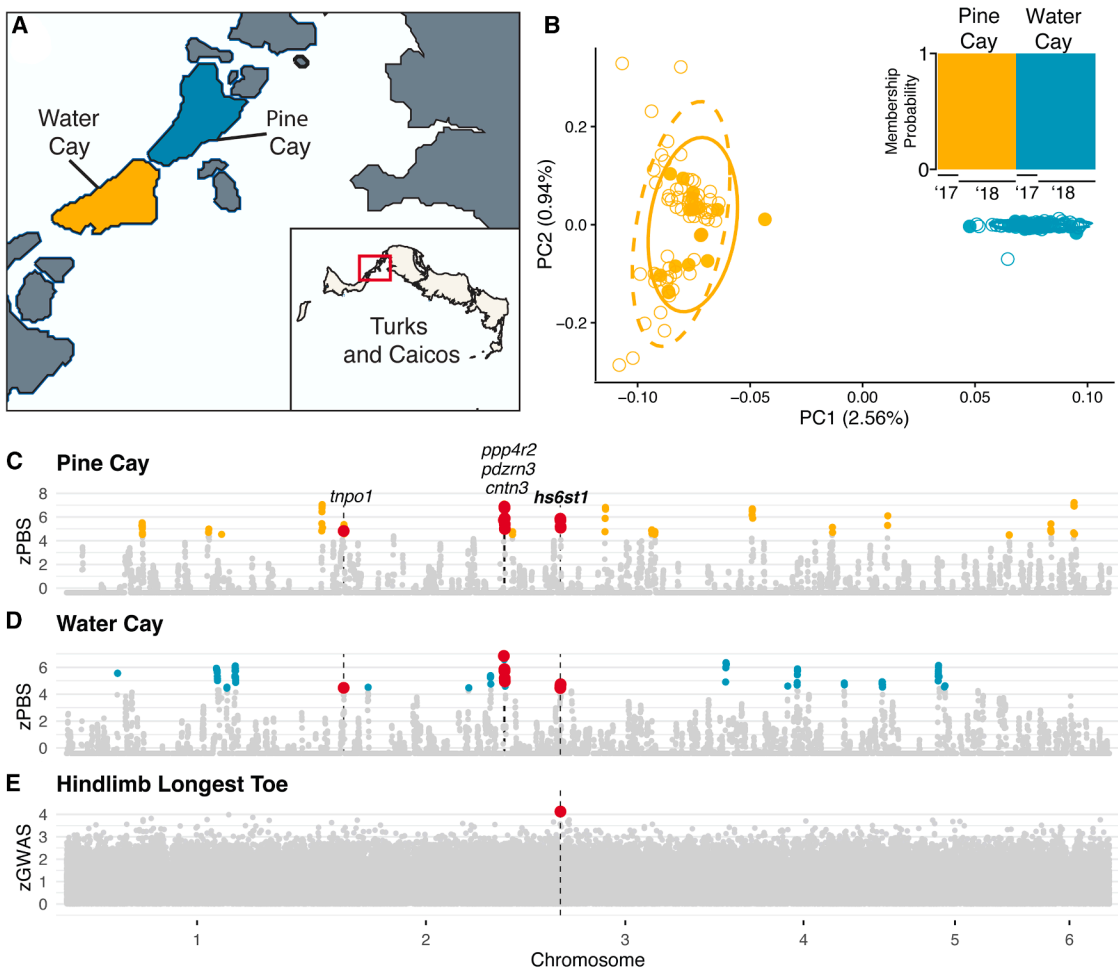


**Figure 1. Hurricane-mediated dispersal and genomic signatures of parallel selection**

(A) We studied populations of *Anolis scriptus* on two islands of the Turks and Caicos (inset), Pine Cay (blue) and Water Cay (gold).

(B) Principal-component analysis of genetic variation reveals significant population structure associated with island-of-origin but no differentiation between pre- (closed circles, solid ellipses) and post-storm (open circles, dotted ellipses) samples. Membership probability assignment displayed no evidence of hurricane-mediated dispersal across islands (inset), setting the stage for the study of parallel responses to the hurricane season.

(C and D) Genomic candidates for selection based on the *Z* score-normalized populations branch statistic.[21] Gray dots represent non-significant (zPBS < 4) regions across each chromosome. (C) Blue dots and (D) gold dots represent significant outliers (zPBS > 4) unique to a single island. Red dots represent significant outliers (zPBS > 4) that are shared between the two islands. This latter class of outliers is considered a strong candidate for event-specific selection.

(E) One candidate locus, *hs6st1*, displays a significant association with the length of the longest hind toe (red dot, zGWAS > 4). Co-localization of parallel divergence signatures across the two islands and phenotypic correlation with a hurricane-responsive phenotype[9] make *hs6st1* a strong candidate as a target for hurricane-mediated interisland parallel selection associated with clinging performance.

See also Figure S1 and Tables S1 and S2.

Therefore, we next searched for genomic evidence of parallel selection across the two islands by calculating the population branch statistic[21] (PBS) at each SNP genome wide (see STAR Methods). To identify regions of the genome displaying accelerated divergence specific to hurricane survivors on each island, we *Z* score normalized PBS scores and independently searched for extreme outliers (zPBS > 4) in each surviving island population. We then compared shared variants between islands to identify shared outliers (SNPs displaying zPBS > 4 in both populations). To further reduce the potential for false positives, we corrected for median branch lengths at all other loci using the population branch excess statistic (PBE) and rescaled our focal branch lengths with respect to outgroup branch lengths using the normalized PBS (PBSn1) (see STAR Methods). Genomic regions in the upper 1% of empirical distributions for at least two of the three statistics (PBS, PBE, and PBSn1) on both islands were retained for further analysis. Only regions supported by both the zPBS analysis and the cross-statistic comparison were taken as strong candidates for parallel targets of hurricane-mediated selection.

Three shared genomic regions on chromosomes 2 and 3 displayed signatures of parallel selection across both surviving populations (Figures 1C and 1D). One genomic region on chromosome 2 overlaps a single gene, Transportin 1 (*tnpo1*), which plays a role in bone mass regulation.[22,23] A second region on chromosome 2 contains a long noncoding RNA

Please cite this article in press as: Vaughn et al., Genomic targets of hurricane-induced selection on clinging performance in an island lizard, Current Biology (2026), https://doi.org/10.1016/j.cub.2026.07.022





(LOC103277965) and three annotated genes (*cntn3*, *pdzn3*, and *ppp4r2*), all of which have known roles in vertebrate musculoskeletal development. Contactin 3 (*cntn3*) has been identified as a tendon-selective gene in rat and human musculoskeletal tissues.[24] Protein Phosphatase 4 Regulatory Subunit 2 (*ppp4r2*) affects the modulation of skeletal muscle via interaction with the survival of motor neuron (SMN) protein and is associated with progressive loss of motor neurons and spinal muscular atrophy.[25,26] Both *cntn3* and *ppp4r2* have been identified as candidate genes for musculoskeletal physiology and race performance in thoroughbred horses.[25,27] PDZ Domain Containing Ring Finger 3 (*pdzn3*) negatively regulates bone morphogenic protein 2 (BMP2)-induced osteoblast differentiation through inhibition of Wnt signaling.[28] The third genomic region on chromosome 3 contains a single gene, heparin sulfate 6-O-sulfotransferase 1 (*hs6st1*), which plays a role in vertebrate limb bud development.[29] Previous studies have shown that experimental knockdown of this locus in chickens resulted in a 20% reduction of the developing limb bud,[29] and *Hs6st1*-deficient mice displayed reduced or missing hind limb tarsi and phalanges, likely resulting from slower bone growth.[30] Taken together, these genomic candidates for parallel selection support the hypothesis that the extreme weather events targeted genes associated with climbing, coordination, and gripping performance in this arboreal species.

## The *hs6st1* locus is associated with rear toe morphology

We next searched for significant associations between each candidate locus and phenotypic traits that displayed parallel hurricane-induced shifts in the surviving population on each island. We performed genome-wide association analyses for each morphological trait displaying parallel shifts in response to the hurricanes using a two-step linear mixed model approach implemented in the GENESIS software package[31] (see STAR Methods). We fit a mixed model for each trait based on a hypothesis of no SNP effect.[31] We then used a linear mixed effects model to determine the significance of association based on the null model. For each model, the first principal component of genetic variation was used as a fixed effect to account for substratification of individuals based on island of origin and genetic relatedness. Phenotypes were size-corrected by quantifying residual values using linear regression against snout-vent length (SVL) after log transformation. Sex was modeled as an additional random variable to account for potential effects of sexual shape dimorphism.[32] Association scores were *Z* score transformed, and we identified SNPs displaying extreme associations with each trait of interest (zGWAS > 4). Among candidate regions, we identified a single-nucleotide variant within *hs6st1* that displayed the strongest genome-wide association with the relative length of the longest rear toe (rear toe IV) (Figure 1E), which was significantly shorter among surviving lizard populations on both islands when compared with their pre-storm counterparts ($\beta \pm$ standard error [SE]: $-0.03 \pm 0.009$; $t_{159} = -3.75$; $p = 0.0002$).[9]

## Co-localized genomic signatures around the *hs6st1* locus

To further test for signatures of selection in this region of chromosome 3, we analyzed 10,299 SNPs from 109 individuals using deep coverage (mean: 182×) capture sequencing of a 2 Mb region surrounding the gene, which included 39 additional loci. To identify the gene(s) within the capture region to most likely be the focal source of the signal detected in genome-wide scans, we assigned SNPs to genes based on genomic overlap and searched for gene-level evidence of co-localization of PBS and genome-wide association study (GWAS) signals (total gene score [TGS]). We estimated a composite score for each SNP using the harmonic mean of *p* values (HMP) from the three focal tests ($PBS_{Pine\ Cay}$, $PBS_{Water\ Cay}$, and $GWAS_{rear\ toe\ length}$) and quantified the proportion of individual tests for which each SNP was within the upper 1% tail of the statistical distribution. Those SNPs reaching nominal support for at least two of the individual component tests were identified as support SNPs within their given gene. TGSs were then calculated as $-\log10(HMP)_{top\ 3\ SNPs} \times (\log10(\text{total \# of support} + 1)/\log10(\text{gene length} + 10))$. As a result, the TGS statistic rewards both the strength of the strongest local cluster within a gene, the consistency of support across individual tests, and the recurrence of support across multiple SNPs while scaling for variation in gene size. Similarly, gene-level PBS and GWAS scores were calculated separately to assess independent evidence for parallelism and trait association, respectively (Figure 2A; see STAR Methods). Genes were then ranked by score in each category. We found that *hs6st1* was the top-ranked gene for parallelism, trait association, and TGS across the 2 Mb region (Figure 2A) and the only gene that was ranked within the top 5 of all three scores (Table S3).

Within *hs6st1*, five SNPs reached the nominal support threshold (Figure 2B), clustering within a 3 kb region of intron 1 that contains multiple adjacent structural elements (Figure 2C). Among these were one miniature inverted-repeat transposable element (DR0008031), two long interspersed nuclear element-1 retrotransposons (DR0007653 and DR0007765), one hAT family DNA transposon (DR0007704), and one GTC(n) trinucleotide simple repetitive element. Each of these structural element classes has been shown to impact gene expression via *cis*-regulation,[33–35] long-range gene regulation,[36] epigenetic modification,[37,38] and/or induction of alternative splicing.[39,40] Analysis of individual supporting SNPs within this genotype block revealed significant genotype-phenotype associations for three variants ($p < 0.01$; Figure 2C). Linear model comparisons estimated that the candidate variants within this genotype block collectively explained 11.58% more total trait variation than the null model ($\Delta R^2$: 0.1158; bootstrap permutation [$n$ = 1,000], $p < 0.05$; Figure 2D). Taken together, these findings support our hypothesis that *hs6st1* is the focal source of the co-localized genomic signatures of parallel divergence and trait association identified in the genome-wide analyses.

## Functional effect of *hs6st1* KO on *Anolis* rear-foot morphology

To test if the *hs6st1* locus has direct influence on hindlimb toe morphology, we conducted a functional validation experiment on an ecomorphologically convergent trunk-ground[41] anole species and the common laboratory model, the brown anole (*Anolis sagrei*). Using CRISPR-Cas9 technology, we performed genetic knockout (KO) of *hs6st1* by introducing indel mutations via non-homologous end joining.[42] We used microinjection of immature oocytes within the ovaries of *A. sagrei* females to produce F0 embryos with

Please cite this article in press as: Vaughn et al., Genomic targets of hurricane-induced selection on clinging performance in an island lizard, Current Biology (2026), https://doi.org/10.1016/j.cub.2026.07.022



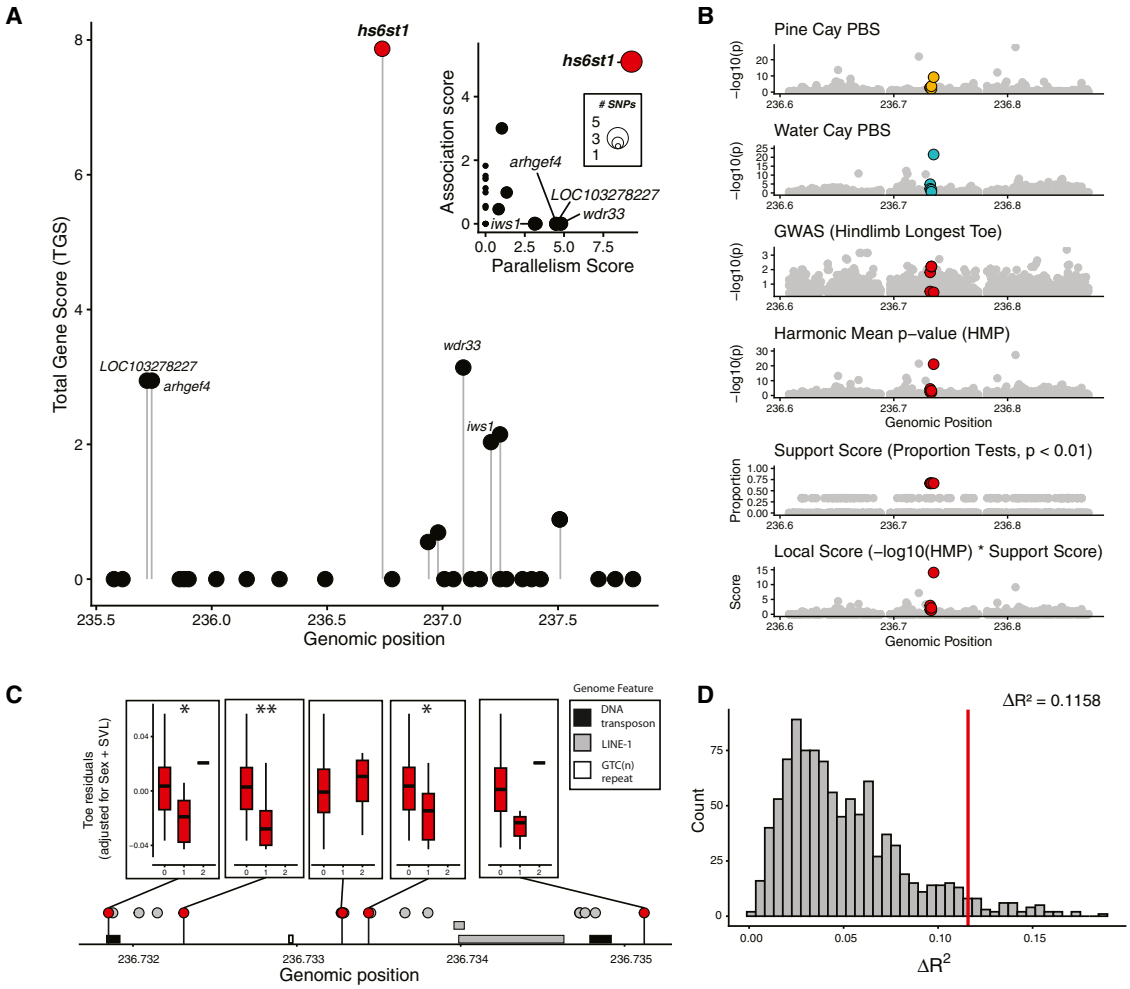


**Figure 2. Finer resolution analyses of co-localized signatures of parallelism and trait association by capture sequencing**

(A) Gene-level integrated evidence for parallelism supports *hs6st1* as the most likely driver of the local genomic signal (inset) as the top-ranked gene for parallelism and trait association across the capture sequence region.

(B) SNP-level analyses of the *hs6st1* locus identified a 3 kb genotype block within intron 1 of the gene driving the gene-level signature.

(C) Five potential regulatory features overlap this region, with 3 of the five individual candidate SNPs displaying significant associations with the relative length of the longest rear toe. Significant genotypic effects are denoted with one ($p < 0.05$) or two ($p < 0.01$) asterisks.

(D) Together, the 3 kb genomic block explains ~11.6% more trait variation than the null model ($\Delta R^2 = 0.1158$, $p < 0.05$).

See also Table S3.

CRISPR-Cas9-induced KO mutations (crispants).[42] Crispant embryos ($n = 5$) were then compared with a panel of homozygous wild-type (WT) *hs6st1* stage-matched embryos ($n = 50$). Images of each embryo were used to obtain SVL and linear measurements of the hindfeet, including the length of the rear toe IV. We then cleared and stained dissected hind limbs from each individual and used Alcian blue 8GX and alizarin red S to stain for cartilage and mineralized bone, respectively. Cartilage area and bone length were quantified for each bone element of the hindlimb, and all phenotypic variables were log10-transformed prior to being analyzed. We found that the *hs6st1* genotype had a significant effect on the length of rear toe IV (ANOVA, $F_{1,\ 50.0} = 5.53$, $p = 0.02$), with crispants displaying reduced toe length compared with their WT counterparts (WT mean = 0.59, KO mean = 0.56).

KOs also displayed allometric divergence in toe length, indicated by a significant genotype * body size interaction (ANOVA, $F_{1,\ 50.0} = 5.43$, $p = 0.02$; Figure 3A). Smaller KO individuals displayed disproportionately smaller elements and greater size dependence of toe length than WT, a pattern consistent with previously described slower bone growth rates in mouse knockdown lines.[30] Individual element analyses of rear toe IV revealed similar allometric relationships for the cartilage area of phalanx 1 (ANOVA, $F_{1,\ 51.0} = 12.9$, $p < 0.001$; Figure 3B) and phalanx 2 ($F_{1,\ 51.0} = 17.0$, $p < 0.001$; Figure 3C). In addition, the *hs6st1* genotype had a significant effect on cartilage area for both phalanx 1 ($F_{1,\ 51.0} = 13.8$, $p < 0.001$) and phalanx 2 ($F_{1,\ 51.0} = 18.2$, $p < 0.001$), with crispants showing reduced cartilage compared with their WT counterparts (phalanx 1: WT mean = −1.23, KO mean = −1.48; phalanx 2: WT mean = −1.43, KO mean = −1.82). A significant reduction in length of the metatarsal ($F_{1,\ 53.0} = 7.1$, $p = 0.01$; Figure 3D), phalanx 1 ($F_{1,\ 52.8} = 6.8$, $p = 0.012$; Figure 3E), and phalanx 2 ($F_{1,\ 53.0} = 6.36$, $p = 0.015$; Figure 3F) was observed in KOs compared with

Please cite this article in press as: Vaughn et al., Genomic targets of hurricane-induced selection on clinging performance in an island lizard, Current Biology (2026), https://doi.org/10.1016/j.cub.2026.07.022



CellPress
OPEN ACCESS

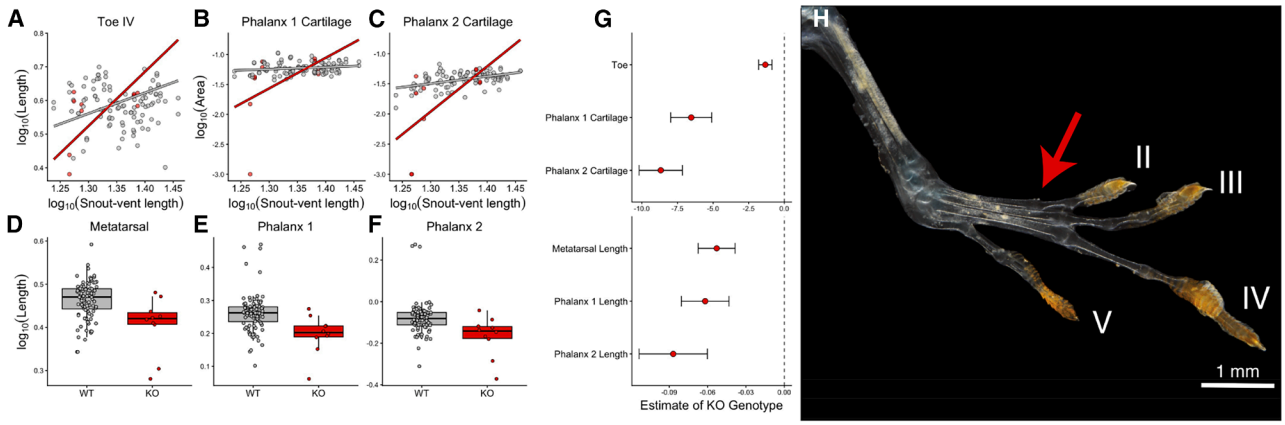


**Figure 3. Functional validation of the *hs6st1* locus**

(A–F) Targeted KO of *hs6st1* in *A. sagrei* resulted in alterations to the scaling and size of the skeletal elements within the hindfoot. KOs showed greater size dependence of the (A) length of the rear toe IV and of the cartilage area within the (B) first and (C) second phalanges of the toe. Analysis of individual element lengths reveals a significant reduction in the length of the (D) metatarsal, (E) first phalanx, and the (F) second phalanx of rear toe IV (all comparisons: ANOVA, $p < 0.05$).

(G) Linear mixed model analysis reveals that the *hs6st1* KO genotype results in significant reductions in trait length and cartilage levels compared with the WT individuals (all comparisons: ANOVA, $p < 0.05$). Scale bar denotes standard error.

(H) A single *hs6st1* KO individual also displayed oligodactyly due to complete agenesis of the 1st toe. Scale bar, 1 mm.

See also Figure S2.

their WT counterparts. Additionally, a single crispant individual displayed complete bilateral agenesis of hind foot digit I (Figure 3H). While the *Hs6st1* locus has been previously demonstrated as necessary for normal limb development in chicken and mouse models,[29,30] our experiments show that the locus is also necessary for distal hindlimb development in anoles. This developmental function further supports our hypothesis that the locus has been a target of hurricane-mediated selection associated with clinging morphology.

## Rear toe morphology contributes significantly to clinging performance under high wind speeds

Next, we directly assessed whether rear toe length provides a significant advantage to the clinging ability of arboreal lizards by conducting a high-wind-speed clinging performance assay under controlled laboratory conditions. We used a custom-fabricated wind shaper (testing section: 30 × 30 cm; Tyoto Robotics, Gatineau, QC, Canada) to generate tropical storm wind speeds (63–118 km/h) in a controlled environment (Figure 4A). Adult male *A. sagrei* ($n$ = 63) were placed head up on the leeward side of a smooth vertical dowel (1.27 cm diameter) 40 cm in front of the wind source. We tested wind speed at this distance using a Kestrel 5500 Weather Meter mounted near the vertical perching dowel (wind speed ± SE: 106.2 ± 0.36 km/h; Figure 4A). Each trial was recorded using a high-speed camera (Sony DSC-RX100M6), and body tracking software (DeepLabCut[43]) recorded changes in lizard body position and clinging release time, which was used as the metric of clinging performance for each trial (see STAR Methods). We then used X-ray measurements to identify morphological associations with variation in clinging performance among individuals.

We found that mean hindlimb clinging time (11.18 s ± 2.10) was significantly shorter than mean forelimb clinging times (22.72 s ± 2.61; Welch's $t$ test: $p$ = 0.0006), with hindlimbs releasing prior to forelimbs in 83.7% of all trials. Further, phalanx 1 of rear toe IV was the only skeletal element with a significant main effect on individual variation in full clinging time, with shorter relative bone lengths associated with longer total clinging times under high-speed wind conditions (linear mixed effects model: estimate = −0.573, df = 30.57, $p$ = 0.042; Figures 4C and 4D). Femur length followed the trend predicted by hurricane-induced selection differentials in the wild[9] but was not significantly correlated with full clinging time (estimate: −0.369, df: 27.57, $p$ = 0.183). Additionally, we found significant interactions between phalanx 1, femur length, and hindlimb extension (phalanx 1 × femur length × hindlimb extension; estimate: 0.92, df = 117.86, $p$ = 0.0007), as well as phalanx 1, metatarsus length, and hindlimb extension (phalanx 1 × metatarsus length × hindlimb extension; estimate: −0.498, df: 115, $p$ = 0.005). Taken together, these results suggest that the relative length of rear toe IV contributes directly to enhanced clinging performance under high-speed wind conditions in the trunk-ground anole ecomorph. Although the two species represent the same *Anolis* ecomorph, to test whether the phenotypic differences between the species may impact the functional relationship of relative fourth toe length, we directly compared phenotypic variation across species. Phenotypes differed significantly (ANOVA, $F_{1,\ 2.21}$ = 31.9, $p$ = 0.024; mean residual fourth toe length, *A. scriptus* = −0.012, *A. sagrei* = 0.030), with *A. sagrei* displaying seven individuals outside of the boundaries of variation displayed by *A. scriptus*. However, removal of these outliers still resulted in the functional relationship between toe length and clinging duration remaining significant (see Figure S3H).

As such, the parallel shifts in rear toe IV length and associated genomic signatures of hurricane-induced selection at the *hs6st1* locus observed in wild populations of the ecomorphologically convergent *A. scriptus* appear to be the product of selection for enhanced clinging ability on vertical perches during hurricane events (for full model results, see Table S4). Longer hindlimb

Please cite this article in press as: Vaughn et al., Genomic targets of hurricane-induced selection on clinging performance in an island lizard, Current Biology (2026), https://doi.org/10.1016/j.cub.2026.07.022



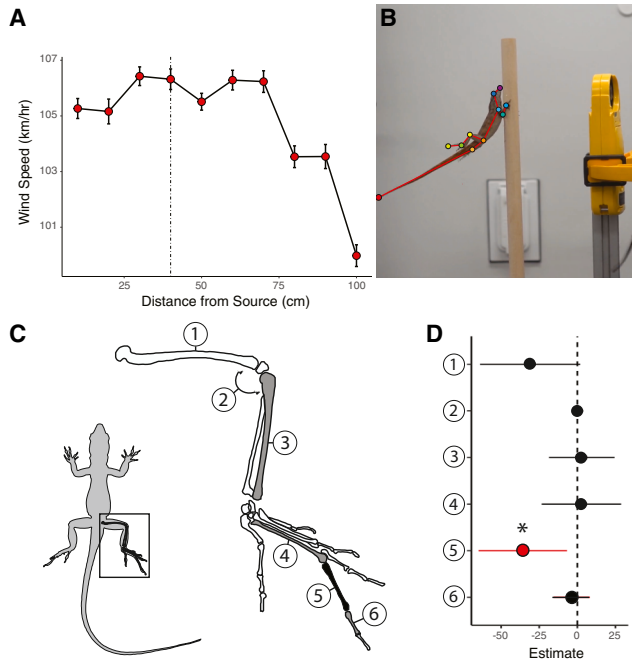


**Figure 4. Effect of hind limb morphology on clinging performance under tropical storm wind speeds**

(A) Controlled high wind-speed clinging trials were performed on *A. sagrei* in the laboratory. Vertical perches were placed 40 cm from the wind source (vertical dotted line). Scale bar denotes standard error.

(B) Body tracking software (highlighted dots) and X-ray data were used to test the contributions of hind limb morphology to overall clinging performance.

(C and D) Linear mixed model analyses of 19 total skeletal elements and their interactive effects show that, among hindlimb elements, only the 1st phalanx of hind limb toe IV (5, colored in red) displays a significant contribution to individual variation in clinging performance, with shorter relative bone lengths associated with longer clinging times. Error bars represent ± 1 SE.

See also Figure S3 and Table S4.

digits have greater surface area and would therefore create greater wind resistance, reducing clinging stability during high wind force events; shorter digits may therefore help mitigate this effect. Consequently, natural variation in digit length and relative element proportions of the toe may provide a valuable substrate for selection to act upon, enabling rapid evolutionary changes in clinging performance under acute high wind conditions. These results align with prior studies showing increased grip strength in other anole species following hurricanes[15] as well as a broader evolutionary trend linking shorter toe lengths to greater clinging ability on rough surfaces among 68 lizard species across 13 squamate families.[44]

## Conclusions

Catastrophic weather events are predicted to increase in both frequency and magnitude in the coming decades,[16,17] imposing selective pressures on wild populations globally. However, the role of such events in shaping evolutionary trajectories in nature has been long debated.[45,46] Unraveling the links between natural selection, ecologically relevant performance, morphology, and genetic variation in the wild is critical for understanding the lasting biological impacts of such events but can be exceedingly difficult to accomplish in field studies. This study demonstrates how extreme weather events can simultaneously alter functional performance, morphological variation, and the genetic underpinnings thereof to produce rapid adaptive responses in the wild. Further, this work demonstrates that genetically distinct populations that endure similar extreme weather events can display rapid parallel responses in complex traits that can be quantified across multiple levels of biological hierarchy. These results have implications for population persistence and conservation management in regions that are increasingly faced with such events, particularly those harboring vulnerable island endemic species with limited geographic distributions.

## RESOURCE AVAILABILITY

### Lead contact

Requests for further information and resources should be directed to and will be fulfilled by the lead contact, Shane C. Campbell-Staton (scampbellstaton@princeton.edu).

### Materials availability

This study did not generate any new, unique reagents.

### Data and code availability

- All raw sequence data associated with this project have been uploaded to NCBI Sequence Read Archive (SRA): BioProject PRJNA1482859.
- Newly collected phenotypic data and code have been uploaded to Zenodo: 10.5281/zenodo.20851209.
- Any additional information required to reanalyze the data reported in this paper is available from the lead contact upon request.

## ACKNOWLEDGMENTS

This material is based upon work supported by the High Meadows Environmental Institute (grant: RQ00505512, awarded to S.C.C.-S. and C.M.D.), the Alfred P. Sloan Foundation (Sloan Research Fellowship in Earth System Science, awarded to S.C.C.-S.), the National Science Foundation grant (DEB-2219279, awarded to S.C.C.-S., and DEB-1927156, awarded to D.B.M.), the National Science Foundation graduate research fellowship (DGE-2039656, awarded to P.L.V.), the National Science Foundation postdoctoral research fellowship (DBI-2109550, awarded to A.D.R., and DBI-2209090, awarded to A.H.G.), and the National Science Foundation grant (IOS-1806420), awarded to J.K. and J.L.

## AUTHOR CONTRIBUTIONS

S.C.C.-S. and C.M.D. conceptualized the study; P.L.V., A.D.R., N.C.R., A.L.R., C.E.S., A.L.I., A.H.G., and S.C.C.-S. performed experiments and formal analyses; P.L.V. and S.C.C.-S. wrote the original draft; P.L.V., C.M.D., A.D.R., N.C.R., D.B.M., A.L.R., C.E.S., A.L.I., A.H.G., A.H., J.K., J.L., and S.C.C.-S. reviewed and edited the manuscript; P.L.V. and S.C.C.-S. prepared the visualizations; S.C.C.-S. and D.B.M. supervised the project; S.C.C.-S. administered the project; P.L.V., C.M.D., A.D.R., D.B.M., A.H.G., J.K., J.L., and S.C.C.-S. acquired funding.

## DECLARATION OF INTERESTS

The authors declare no competing interests.

## STAR★METHODS

Detailed methods are provided in the online version of this paper and include the following:

- KEY RESOURCES TABLE
- EXPERIMENTAL MODEL AND STUDY PARTICIPANT DETAILS

## SUPPLEMENTAL INFORMATION

Supplemental information can be found online at https://doi.org/10.1016/j.cub.2026.07.022.

Received: July 23, 2025
Revised: May 5, 2026
Accepted: July 9, 2026

## REFERENCES


1. Grant, P.R., and Grant, B.R. (2002). Unpredictable Evolution in a 30-Year Study of Darwin's Finches. Science *296*, 707–711. https://doi.org/10.1126/science.1070315.
2. Campbell-Staton, S.C., Cheviron, Z.A., Rochette, N., Catchen, J., Losos, J.B., and Edwards, S.V. (2017). Winter storms drive rapid phenotypic, regulatory, and genomic shifts in the green anole lizard. Science *357*, 495–498. https://doi.org/10.1126/science.aam5512.
3. Heartsill Scalley, T., Scatena, F.N., Lugo, A.E., Moya, S., and Estrada Ruiz, C.R. (2010). Changes in Structure, Composition, and Nutrients During 15 Yr of Hurricane-Induced Succession in a Subtropical Wet Forest in Puerto Rico. Biotropica *42*, 455–463. https://doi.org/10.1111/j.1744-7429.2009.00609.x.
4. Tanner, E.V.J., Kapos, V., and Healey, J.R. (1991). Hurricane Effects on Forest Ecosystems in the Caribbean. Biotropica *23*, 513. https://doi.org/10.2307/2388274.
5. Walker, R.H., Hutchinson, M.C., Becker, J.A., Daskin, J.H., Gaynor, K.M., Palmer, M.S., Gonçalves, D.D., Stalmans, M.E., Denlinger, J., Bouley, P., et al. (2023). Trait-based sensitivity of large mammals to a catastrophic tropical cyclone. Nature *623*, 757–764. https://doi.org/10.1038/s41586-023-06722-0.
6. Fleming, T.H., and Murray, K.L. (2009). Population and Genetic Consequences of Hurricanes for Three Species of West Indian Phyllostomid Bats. Biotropica *41*, 250–256. https://doi.org/10.1111/j.1744-7429.2008.00466.x.
7. Pagán, J.A., Veríssimo, A., Sikkel, P.C., and Xavier, R. (2020). Hurricane-induced disturbance increases genetic diversity and population admixture of the direct-brooding isopod, Gnathia marleyi. Sci. Rep. *10*, 8649. https://doi.org/10.1038/s41598-020-64779-7.
8. Bumpus, H.C. (1899). The elimination of the unfit as illustrated by the introduced House Sparrow Passer domesticus (Gin), pp. 209–226. https://books.google.co.in/books/about/The_Elimination_of_the_Unfit_as_Illustra.html?id=zvjgjgEACAAJ&redir_esc=y.
9. Donihue, C.M., Herrel, A., Fabre, A.-C., Kamath, A., Geneva, A.J., Schoener, T.W., Kolbe, J.J., and Losos, J.B. (2018). Hurricane-induced selection on the morphology of an island lizard. Nature *560*, 88–91. https://doi.org/10.1038/s41586-018-0352-3.
10. Donihue, C.M., Kowaleski, A.M., Losos, J.B., Algar, A.C., Baeckens, S., Buchkowski, R.W., Fabre, A.-C., Frank, H.K., Geneva, A.J., Reynolds, R.G., et al. (2020). Hurricane effects on Neotropical lizards span geographic and phylogenetic scales. Proc. Natl. Acad. Sci. USA *117*, 10429–10434. https://doi.org/10.1073/pnas.2000801117.
11. Kolbe, J.J., Giery, S.T., Petherick, A.S., Losos, J.B., and Bock, D.G. (2025). Morphological and genomic responses to hurricanes arise and persist during a biological invasion. Proc. Natl. Acad. Sci. USA *122*, e2517322122. https://doi.org/10.1073/pnas.2517322122.
12. DiPaolo, E.C.C., and Kolbe, J.J. (2023). Blowing in the wind: Experimental assessment of clinging performance and behaviour in *Anolis* lizards during hurricane-force winds. Funct. Ecol. *37*, 638–647. https://doi.org/10.1111/1365-2435.14260.
13. Rodríguez-Trelles, F., Tarrío, R., and Santos, M. (2013). Genome-wide evolutionary response to a heat wave in *Drosophila*. Biol. Lett. *9*, 20130228. https://doi.org/10.1098/rsbl.2013.0228.
14. Brown, C.R., and Brown, M.B. (1998). Intense natural selection on body size and wing and tail asymmetry in cliff swallows during severe weather. Evolution *52*, 1461–1475. https://doi.org/10.1111/j.1558-5646.1998.tb02027.x.
15. Dufour, C.M.S., Donihue, C.M., Losos, J.B., and Herrel, A. (2019). Parallel increases in grip strength in two species of *Anolis* lizards after a major hurricane on Dominica. J. Zool. *309*, 77–83. https://doi.org/10.1111/jzo.12685.
16. Sobel, A.H., Camargo, S.J., Hall, T.M., Lee, C.-Y., Tippett, M.K., and Wing, A.A. (2016). Human influence on tropical cyclone intensity. Science *353*, 242–246. https://doi.org/10.1126/science.aaf6574.
17. Holland, G., and Bruyère, C.L. (2014). Recent intense hurricane response to global climate change. Clim. Dyn. *42*, 617–627. https://doi.org/10.1007/s00382-013-1713-0.
18. Maxwell, S.L., Butt, N., Maron, M., McAlpine, C.A., Chapman, S., Ullmann, A., Segan, D.B., and Watson, J.E.M. (2019). Conservation implications of ecological responses to extreme weather and climate events. Divers. Distrib. *25*, 613–625. https://doi.org/10.1111/ddi.12878.
19. Andrews, K.R., Good, J.M., Miller, M.R., Luikart, G., and Hohenlohe, P.A. (2016). Harnessing the power of RADseq for ecological and evolutionary genomics. Nat. Rev. Genet. *17*, 81–92. https://doi.org/10.1038/nrg.2015.28.
20. Baird, N.A., Etter, P.D., Atwood, T.S., Currey, M.C., Shiver, A.L., Lewis, Z.A., Selker, E.U., Cresko, W.A., and Johnson, E.A. (2008). Rapid SNP Discovery and Genetic Mapping Using Sequenced RAD Markers. PLoS One *3*, e3376. https://doi.org/10.1371/journal.pone.0003376.
21. Yi, X., Liang, Y., Huerta-Sanchez, E., Jin, X., Cuo, Z.X.P., Pool, J.E., Xu, X., Jiang, H., Vinckenbosch, N., Korneliussen, T.S., et al. (2010). Sequencing of 50 Human Exomes Reveals Adaptation to High Altitude. Science *329*, 75–78. https://doi.org/10.1126/science.1190371.
22. Sun, L., Tamma, R., Yuen, T., Colaianni, G., Ji, Y., Cuscito, C., Bailey, J., Dhawan, S., Lu, P., Calvano, C.D., et al. (2016). Functions of vasopressin and oxytocin in bone mass regulation. Proc. Natl. Acad. Sci. USA *113*, 164–169. https://doi.org/10.1073/pnas.1523762113.
23. Di Benedetto, A., Sun, L., Zambonin, C.G., Tamma, R., Nico, B., Calvano, C.D., Colaianni, G., Ji, Y., Mori, G., Grano, M., et al. (2014). Osteoblast regulation via ligand-activated nuclear trafficking of the oxytocin receptor. Proc. Natl. Acad. Sci. USA *111*, 16502–16507. https://doi.org/10.1073/pnas.1419349111.
24. Jelinsky, S.A., Archambault, J., Li, L., and Seeherman, H. (2010). Tendon-selective genes identified from rat and human musculoskeletal tissues. J. Orthop. Res. *28*, 289–297. https://doi.org/10.1002/jor.20999.
25. Littiere, T.O., Castro, G.H.F., Rodriguez, M.D.P.R., Bonafé, C.M., Magalhães, A.F.B., Faleiros, R.R., Vieira, J.I.G., Santos, C.G., and Verardo, L.L. (2020). Identification and Functional Annotation of Genes Related to Horses' Performance: From GWAS to Post-GWAS. Animals *10*, 1173. https://doi.org/10.3390/ani10071173.
26. Bosio, Y., Berto, G., Camera, P., Bianchi, F., Ambrogio, C., Claus, P., and Di Cunto, F. (2012). PPP4R2 regulates neuronal cell differentiation and survival, functionally cooperating with SMN. Eur. J. Cell Biol. *91*, 662–674. https://doi.org/10.1016/j.ejcb.2012.03.002.

27. Shin, D.-H., Lee, J.W., Park, J.-E., Choi, I.-Y., Oh, H.-S., Kim, H.J., and Kim, H. (2015). Multiple Genes Related to Muscle Identified through a Joint Analysis of a Two-stage Genome-wide Association Study for Racing Performance of 1,156 Thoroughbreds. Asian-Australas. J. Anim. Sci. *28*, 771–781. https://doi.org/10.5713/ajas.14.0008.

28. Honda, T., Yamamoto, H., Ishii, A., and Inui, M. (2010). PDZRN3 Negatively Regulates BMP-2–induced Osteoblast Differentiation through Inhibition of Wnt Signaling. Mol. Biol. Cell *21*, 3269–3277. https://doi.org/10.1091/mbc.e10-02-0117.

29. Kobayashi, T., Habuchi, H., Nogami, K., Ashikari-Hada, S., Tamura, K., Ide, H., and Kimata, K. (2010). Functional analysis of chick heparan sulfate 6-*O*-sulfotransferases in limb bud development. Dev. Growth Differ. *52*, 146–156. https://doi.org/10.1111/j.1440-169X.2009.01148.x.

30. Habuchi, H., Nagai, N., Sugaya, N., Atsumi, F., Stevens, R.L., and Kimata, K. (2007). Mice Deficient in Heparan Sulfate 6-O-Sulfotransferase-1 Exhibit Defective Heparan Sulfate Biosynthesis, Abnormal Placentation, and Late Embryonic Lethality. J. Biol. Chem. *282*, 15578–15588. https://doi.org/10.1074/jbc.M607434200.

31. Gogarten, S.M., Sofer, T., Chen, H., Yu, C., Brody, J.A., Thornton, T.A., Rice, K.M., and Conomos, M.P. (2019). Genetic association testing using the GENESIS R/Bioconductor package. Bioinformatics *35*, 5346–5348. https://doi.org/10.1093/bioinformatics/btz567.

32. Butler, M.A., Sawyer, S.A., and Losos, J.B. (2007). Sexual dimorphism and adaptive radiation in Anolis lizards. Nature *447*, 202–205. https://doi.org/10.1038/nature05774.

33. Chen, L., Yang, Q., Zhang, Y., and Sun, Y. (2025). Miniature-inverted-repeat transposable elements contribute to phenotypic variation regulation of rice induced by space environment. Front. Plant Sci. *15*, 1446383. https://doi.org/10.3389/fpls.2024.1446383.

34. Wei, L., Gu, L., Song, X., Cui, X., Lu, Z., Zhou, M., Wang, L., Hu, F., Zhai, J., Meyers, B.C., et al. (2014). Dicer-like 3 produces transposable element-associated 24-nt siRNAs that control agricultural traits in rice. Proc. Natl. Acad. Sci. USA *111*, 3877–3882. https://doi.org/10.1073/pnas.1318131111.

35. Shen, J., Liu, J., Xie, K., Xing, F., Xiong, F., Xiao, J., Li, X., and Xiong, L. (2017). Translational repression by a miniature inverted-repeat transposable element in the 3′ untranslated region. Nat. Commun. *8*, 14651. https://doi.org/10.1038/ncomms14651.

36. Li, X., Bie, L., Wang, Y., Hong, Y., Zhou, Z., Fan, Y., Yan, X., Tao, Y., Huang, C., Zhang, Y., et al. (2024). LINE-1 transcription activates long-range gene expression. Nat. Genet. *56*, 1494–1502. https://doi.org/10.1038/s41588-024-01789-5.

37. Xu, P., Chen, H., Hu, J., and Cai, W. (2021). Potential evidence for transgenerational epigenetic memory in Arabidopsis thaliana following spaceflight. Commun. Biol. *4*, 835. https://doi.org/10.1038/s42003-021-02342-4.

38. Xu, P., Chen, H., Jin, J., and Cai, W. (2018). Single-base resolution methylome analysis shows epigenetic changes in Arabidopsis seedlings exposed to microgravity spaceflight conditions on board the SJ-10 recoverable satellite. npj Microgravity *4*, 12. https://doi.org/10.1038/s41526-018-0046-z.

39. Nakazaki, T., Okumoto, Y., Horibata, A., Yamahira, S., Teraishi, M., Nishida, H., Inoue, H., and Tanisaka, T. (2003). Mobilization of a transposon in the rice genome. Nature *421*, 170–172. https://doi.org/10.1038/nature01219.

40. Naito, K., Zhang, F., Tsukiyama, T., Saito, H., Hancock, C.N., Richardson, A.O., Okumoto, Y., Tanisaka, T., and Wessler, S.R. (2009). Unexpected consequences of a sudden and massive transposon amplification on rice gene expression. Nature *461*, 1130–1134. https://doi.org/10.1038/nature08479.

41. Losos, J.B. (2011). Lizards in an Evolutionary Tree: Ecology and Adaptive Radiation of Anoles (University of California Press).

42. Rasys, A.M., Park, S., Ball, R.E., Alcala, A.J., Lauderdale, J.D., and Menke, D.B. (2019). CRISPR-Cas9 Gene Editing in Lizards through Microinjection of Unfertilized Oocytes. Cell Rep. *28*, 2288–2292.e3. https://doi.org/10.1016/j.celrep.2019.07.089.

43. Mathis, A., Mamidanna, P., Cury, K.M., Abe, T., Murthy, V.N., Mathis, M.W., and Bethge, M. (2018). DeepLabCut: markerless pose estimation of user-defined body parts with deep learning. Nat. Neurosci. *21*, 1281–1289. https://doi.org/10.1038/s41593-018-0209-y.

44. Zani. (2000). The comparative evolution of lizard claw and toe morphology and clinging performance. J. Evol. Biol. *13*, 316–325. https://doi.org/10.1046/j.1420-9101.2000.00166.x.

45. Gould, S.J. (1985). The paradox of the first tier: an agenda for paleobiology. Paleobiology *11*, 2–12. https://doi.org/10.1017/S0094837300011350.

46. O'Donald, P. (1973). A further analysis of Bumpus' data: the intensity of natural selection. Evolution *27*, 398–404. https://doi.org/10.1111/j.1558-5646.1973.tb00686.x.

47. Rochette, N.C., Rivera-Colón, A.G., and Catchen, J.M. (2019). Stacks 2: Analytical methods for paired-end sequencing improve RADseq-based population genomics. Mol. Ecol. *28*, 4737–4754. https://doi.org/10.1111/mec.15253.

48. Li, H. (2018). Minimap2: pairwise alignment for nucleotide sequences. Bioinformatics *34*, 3094–3100. https://doi.org/10.1093/bioinformatics/bty191.

49. Mirchandani, C.D., Shultz, A.J., Thomas, G.W.C., Smith, S.J., Baylis, M., Arnold, B., Corbett-Detig, R., Enbody, E., and Sackton, T.B. (2024). A Fast, Reproducible, High-throughput Variant Calling Workflow for Population Genomics. Mol. Biol. Evol. *41*, msad270. https://doi.org/10.1093/molbev/msad270.

50. Chen, S., Zhou, Y., Chen, Y., and Gu, J. (2018). fastp: an ultra-fast all-in-one FASTQ preprocessor. Bioinformatics *34*, i884–i890. https://doi.org/10.1093/bioinformatics/bty560.

51. Li, H., and Durbin, R. (2009). Fast and accurate short read alignment with Burrows–Wheeler transform. Bioinformatics *25*, 1754–1760. https://doi.org/10.1093/bioinformatics/btp324.

52. Van der Auwera, G.A., Carneiro, M.O., Hartl, C., Poplin, R., Del Angel, G., Levy-Moonshine, A., Jordan, T., Shakir, K., Roazen, D., Thibault, J., et al. (2013). From FastQ data to high-confidence variant calls: the genome analysis toolkit best practices pipeline. Curr. Protoc. Bioinform. *43*. 11.10.1–11.10.33. https://doi.org/10.1002/0471250953.bi1110s43.

53. Danecek, P., Auton, A., Abecasis, G., Albers, C.A., Banks, E., DePristo, M.A., Handsaker, R.E., Lunter, G., Marth, G.T., Sherry, S.T., et al. (2011). The variant call format and VCFtools. Bioinformatics *27*, 2156–2158. https://doi.org/10.1093/bioinformatics/btr330.

54. Concordet, J.-P., and Haeussler, M. (2018). CRISPOR: intuitive guide selection for CRISPR/Cas9 genome editing experiments and screens. Nucleic Acids Res. *46*, W242–W245. https://doi.org/10.1093/nar/gky354.

55. Bloh, K., Kanchana, R., Bialk, P., Banas, K., Zhang, Z., Yoo, B.-C., and Kmiec, E.B. (2021). Deconvolution of Complex DNA Repair (DECODR): Establishing a Novel Deconvolution Algorithm for Comprehensive Analysis of CRISPR-Edited Sanger Sequencing Data. CRISPR J. *4*, 120–131. https://doi.org/10.1089/crispr.2020.0022.

56. Hwang, G.-H., Vyshedskiy, B., Barry, T., Zeng, J., Manis, J.P., Shimamura, A., Bauer, D.E., and Pinello, L. (2025). Analyzing long-read CRISPR experiments with CRISPRLungo. Preprint at bioRxiv. https://doi.org/10.1101/2025.10.21.683786.

57. Kearse, M., Moir, R., Wilson, A., Stones-Havas, S., Cheung, M., Sturrock, S., Buxton, S., Cooper, A., Markowitz, S., Duran, C., et al. (2012). Geneious Basic: An integrated and extendable desktop software platform for the organization and analysis of sequence data. Bioinformatics *28*, 1647–1649. https://doi.org/10.1093/bioinformatics/bts199.

58. Schindelin, J., Arganda-Carreras, I., Frise, E., Kaynig, V., Longair, M., Pietzsch, T., Preibisch, S., Rueden, C., Saalfeld, S., Schmid, B., et al. (2012). Fiji: an open-source platform for biological-image analysis. Nat. Methods *9*, 676–682. https://doi.org/10.1038/nmeth.2019.

59. Jombart, T. (2008). *adegenet*: A R package for the multivariate analysis of genetic markers. Bioinformatics *24*, 1403–1405. https://doi.org/10.1093/bioinformatics/btn129.

60. Purcell, S., Neale, B., Todd-Brown, K., Thomas, L., Ferreira, M.A.R., Bender, D., Maller, J., Sklar, P., De Bakker, P.I.W., Daly, M.J., et al. (2007). PLINK: A tool set for whole-genome association and population-based linkage analyses. Am. J. Hum. Genet. *81*, 559–575. https://doi.org/10.1086/519795.

61. Etter, P.D., Preston, J.L., Bassham, S., Cresko, W.A., and Johnson, E.A. (2011). Local De Novo Assembly of RAD Paired-End Contigs Using Short Sequencing Reads. PLoS One *6*, e18561. https://doi.org/10.1371/journal.pone.0018561.

62. Garcia-Elfring, A., Sabin, C.E., Iouchmanov, A.L., Roffey, H.L., Samudra, S.P., Alcala, A.J., Osman, R.S., Lauderdale, J.D., Hendry, A.P., Menke, D.B., et al. (2023). Piebaldism and chromatophore development in reptiles are linked to the tfec gene. Curr. Biol. *33*, 755–763.e3. https://doi.org/10.1016/j.cub.2023.01.004.

63. Griffing, A.H., Gamble, T., Bauer, A.M., and Russell, A.P. (2022). Ontogeny of the paraphalanges and derived phalanges of *Hemidactylus turcicus* (Squamata: Gekkonidae). J. Anat. *241*, 1039–1053. https://doi.org/10.1111/joa.13735.

64. Wassersug, R.J. (1976). A procedure for differential staining of cartilage and bone in whole formalin-fixed vertebrates. Stain Technol. *51*, 131–134. https://doi.org/10.3109/10520297609116684.

65. Hanken, J. (1981). The visible skeleton. Funct. Photogr. *16*, 22–26. https://hankenlab.oeb.harvard.edu/publications/visible-skeleton.

66. R Core Team (2022). R: A language and environment for statistical computing (R Foundation for Statistical Computing).

67. Yassin, A., Debat, V., Bastide, H., Gidaszewski, N., David, J.R., and Pool, J.E. (2016). Recurrent specialization on a toxic fruit in an island *Drosophila* population. Proc. Natl. Acad. Sci. USA *113*, 4771–4776. https://doi.org/10.1073/pnas.1522559113.

68. Malaspinas, A.-S., Westaway, M.C., Muller, C., Sousa, V.C., Lao, O., Alves, I., Bergström, A., Athanasiadis, G., Cheng, J.Y., Crawford, J.E., et al. (2016). A genomic history of Aboriginal Australia. Nature *538*, 207–214. https://doi.org/10.1038/nature18299.

69. Shpak, M., Lawrence, K.N., and Pool, J.E. (2024). The Precision and Power of Population Branch Statistics in Identifying the Genomic Signatures of Local Adaptation. Preprint at bioRxiv. https://doi.org/10.1101/2024.05.14.594139.

Please cite this article in press as: Vaughn et al., Genomic targets of hurricane-induced selection on clinging performance in an island lizard, Current Biology (2026), https://doi.org/10.1016/j.cub.2026.07.022



## STAR★METHODS

### KEY RESOURCES TABLE

| REAGENT or RESOURCE | SOURCE | IDENTIFIER |
|---|---|---|
| **Biological samples** | | |
| Silver Key Anole (*Anolis scriptus*) | This paper | N/A |
| **Chemicals, peptides, and recombinant proteins** | | |
| Alcian Blue 8 GX | Fisher | AAJ6012209 |
| Alizarin Red S | Fisher | AC400480250 |
| Trypsin from Porcine Pancreas | Sigma | T4799-25g |
| Potassium hydroxide (KOH) | Sigma Aldrich | P1767-500G |
| Glycerol | Research Products International | G22025-4.0 |
| **Critical commercial assays** | | |
| Custom Capture Array | Arbor Daicel Biosciences | N/A |
| DNeasy® Blood & Tissue Kit | Qiagen | 69504 |
| Invitrogen Qubit dsDNA HS Assay kit | Invitrogen | Q32850 |
| **Oligonucleotides** | | |
| *hs6st1* CRISPR gRNA | Synthego | GGCGCACGTTCTGGACCAGG |
| *hs6st1* CRISPR gRNA | Synthego | TCGAGGTGCCCTGCGACTGC |
| **Software and algorithms** | | |
| Stacks v2.5 | Rochette et al.[47] | https://catchenlab.life.illinois.edu/stacks/ |
| Minimap2 | Li[48] | https://github.com/lh3/minimap2 |
| snpArcher v1.0 workflow | Mirchandani et al.[49] | https://snparcher.github.io/ |
| fastp v0.20.1 | Chen et al.[50] | https://github.com/opengene/fastp |
| bwa-mem v0.7.17 | Li and Durbin[51] | https://github.com/lh3/BWA |
| GATK v4.1.8 | Van der Auwera et al.[52] | https://gatk.broadinstitute.org/hc/en-us |
| vcftools v0.1.17 | Danecek[53] | https://vcftools.github.io/index.html |
| CRISPOR 4.4 | Concordet and Haeussler[54] | http://crispor.tefor.net/ |
| DECODR | Bloh et al.[55] | https://decodr.org/ |
| CRISPRLungo | Hwang et al.[56] | https://github.com/pinellolab/CRISPRlungo |
| Geneious Prime v2025.2.2 | Kearse et al.[57] | https://www.geneious.com/ |
| Fiji V2.14 | Schindelin et al.[58] | https://imagej.net/software/fiji/ |
| adegenet R package | Jombart[59] | https://cran.r-project.org/web/packages/adegenet/index.html |
| PLINK v1.90b3.45 | Purcell et al.[60] | https://www.cog-genomics.org/plink/ |
| GENESIS R package | Gogarten et al.[31] | https://bioconductor.org/packages/release/bioc/html/GENESIS.html |
| DeepLabCut v2.3.11 | Mathis et al.[43] | https://github.com/deeplabcut/deeplabcut |
| **Other** | | |
| Sony DSC-RX100M6 digital camera | Sony Electronics | Sony RX100 VI |
| Custom Portable Digital X-ray machine | Kodex | N/A |
| Custom Windshaper Fan System | Tyto Robotics | N/A |
| Olympus SZX7 stereoscope | Marshall Scientific | OL-SZX7 |
| DFK 37BUX250 microscope camera | Imaging Source | DFK 37BUX250 |
| **Deposited data** | | |
| *Anolis scriptus* restriction-site associated sequencing and targeted capture sequencing data in fastq format | This paper | NCBI SRA BioProject PRJNA1482859 |
| Raw phenotypic data | This paper | Zenodo: 10.5281/zenodo.20851209 |

(*Continued on next page*)

Please cite this article in press as: Vaughn et al., Genomic targets of hurricane-induced selection on clinging performance in an island lizard, Current Biology (2026), https://doi.org/10.1016/j.cub.2026.07.022



CellPress
OPEN ACCESS

*Continued*

| REAGENT or RESOURCE | SOURCE | IDENTIFIER |
|---|---|---|
| *Anolis carolinensis* reference genome (AnoCar2.0) | Broad Institute | https://www.ncbi.nlm.nih.gov/datasets/genome/GCF_000090745.1/ |
| *Anolis carolinensis* reference genome (rAnoCar3.1.pri) | Louisiana State University | https://www.ncbi.nlm.nih.gov/datasets/genome/GCF_035594765.1/ |
| *Anolis sagrei* reference genome (AnoSag2.1) | Rutgers University | https://www.ncbi.nlm.nih.gov/datasets/genome/GCF_025583915.1/ |

## EXPERIMENTAL MODEL AND STUDY PARTICIPANT DETAILS

Lizard measurements and tissues were collected as outlined in Donihue et al.[9] Briefly, the initial survey and tissue collection of *Anolis scriptus* on Pine Cay and Water Cay (Turks and Caicos) occurred from August 28, 2017 to September 4, 2017. Hurricanes Irma and Maria hit Turks and Caicos on September 8 and September 22, 2017, respectively. The post-hurricane data and tissue collections occurred from October 16, 2018 to October 20, 2018. Lizard populations were sampled across a ~2-km long transect. Lizards were captured by noose and pole. A total of 159 *A. scriptus* individuals were collected and used for this study, corresponding to 92 males (pre-storm; Pine Cay = 10, Water Cay = 11, post-storm; Pine Cay = 33, Water Cay = 38) and 67 females (pre-storm; Pine Cay = 6, Water Cay = 8, post-storm; Pine Cay = 29, Water Cay = 24). During each survey, digital calipers (Mitutoyo 500-752) were used to measure morphological variables (snout-to-vent length, and length of the humerus, radius, metacarpal, longest forelimb toe, femur, tibia, metatarsal and longest hindlimb toe) for each lizard, which were subsequently released at their point of initial capture unharmed. All collection procedures were approved by Harvard IACUC (26-11).

Additionally, we collected 62 adult male *Anolis sagrei* from Miami, Florida from August 7$^{th}$–10$^{th}$, 2023 to support the high wind clinging performance analyses. Lizards were transported back to Princeton University and singly housed and fed crickets and mealworms three times a week, while water was provided *ad libitum*. Performance experiments were conducted from October 17$^{th}$–October 20$^{th}$, 2023. Lizards were placed with their head oriented upwards on a 1.27 cm diameter wooden dowel positioned 40cm from the wind source which generated mean wind speeds of 106.2 km/hr. Soft padding was provided to ensure the safety of the individual after falling off the perch. Each individual was tested three times in quick succession to ensure maximum performance was reached. All experimental procedures were approved by Princeton IACUC (#3119).

## METHOD DETAILS

### RADseq DNA extraction, preparation, sequencing, and quality filtering

Genomic DNA was extracted from all *Anolis scriptus* tissue samples using the DNeasy® Blood & Tissue Kit (Qiagen) and quantified using a Qubit fluorometer (Life Technologies). RAD-seq libraries were prepared and sequenced by Floragenex, Inc. (Portland Oregon, USA) using a protocol adapted from Baird et al.[20] and Etter et al.[61] An average of 280ng of genomic DNA per sample was digested with *SbfI*-HF (NEB) for 60 min at 37°C in a 15μL reaction, followed by heat inactivation for 20 min at 80°C. Custom P1 adapters comprising 10bp barcodes were ligated to each sample using T4 DNA Ligase (Enzymatics, Inc) at room temperature for 20 min, following by heat inactivation for 20 min at 65°C. Samples were then pooled, sheared with a Bioruptor (Diagenode), purified and concentrated with a MinElute Reaction Cleanup Kit (Qiagen). DNA fragments holding inserts in the 150-750bp range were isolated from a 1.5% agarose, 0.5x TBE gel using a MinElute Gel Extraction Kit (Qiagen) and polished with an End Repair/dA-Tailing module (NEB). After subsequent purification, custom P2 Y-adapters were ligated to the DNA fragments at room temperature. The ligated product was purified and quantified using a Qubit Fluorometer with the dsDNA HS assay kit (Invitrogen/Thermo Fisher). Libraries were amplified for 18 cycles and amplification reactions were pooled. Each library was cleaned and concentrated with a PCR Purification Kit (Qiagen), and size selected as previously described. The final libraries were quantified on an Agilent Bioanalyzer and sequenced 2×100bp on an Illumina HighSeq-4000.

Sequencing data for each library were analyzed separately using *Stacks* v2.5.[47] Raw reads were processed and demultiplexed using the PROCESS_RADTAGS program. RAD loci were assembled de novo using the denovo_map.pl script. The mismatch parameters M and n were set to 5. We identified and removed PCR duplicates (–-rm-pcr-duplicates) and selected only loci present in over half the samples in the library (using the flag -X 'gstacks: –dbg-min-loc-spls'). The final loci and variant sites were exported in VCF format using the POPULATIONS program, keeping variants genotyped in at least 80% of samples (–r 0.8). RAD libraries using the Stacks v.2.5 pipeline.[47] We identified and removed PCR duplicates (–rm-pcr-duplicates) and selected only loci present in a majority of samples (flag -X "gstacks: –dbg-min-loc-spls" was set to half the number of samples in each library). Assembled RAD loci (contig length ~600bp) were mapped to the reference *A. carolinensis* genome (AnoCar2.0, retrieved from Ensembl) using Minimap2 v2.17[48] with default nanopore ('map-ont') parameters, retaining alignments with qualities greater than 20. These alignments were then fed to STACKS's "integrate alignments" module to convert the *de novo* SNP generated above to *A. carolinensis* coordinates. Finally, the populations program was used to export variants genotyped in at least 50% of samples (-r 0.5) in VCF format.

Please cite this article in press as: Vaughn et al., Genomic targets of hurricane-induced selection on clinging performance in an island lizard, Current Biology (2026), https://doi.org/10.1016/j.cub.2026.07.022



### Capture array preparation, sequencing, and quality filtering

We designed a custom capture array (myBaits® Custom Hybridization Capture Kits from Arbor Daicel) targeting a ~2 Mb region on *Anolis carolinensis* chromosome 3 (rAnoCar3.1; Chromosome 3: 235,882,675 - 237,942,595), centered on the *hs6st1* gene with ~1 Mb flanking sequence on each side. Baits were designed by Arbor Biosciences using 80nt probes at ~2× tiling density, yielding 61,727 initial candidate baits. Using the Basic Local Alignment Search Tool (BLAST), candidates were filtered against both versions of the reference genome (AnoCar3.1 and AnoCar2.0) to remove probes matching over-represented loci or the mitochondrial genome. This resulted in ~20,000 baits passing the filtering criteria. A subset of 109 individuals from the RADseq dataset were selected for capture sequencing using the "Standard capture protocol" as described in their myBaits_Manual_v5.03.pdf. Individuals were chosen due to having sufficient amounts of DNA remaining after RADseq. Libraries were pooled and subject to in-solution hybridization capture following the Arbor Biosciences myBaits protocol. Briefly, denatured libraries were hybridized with the baits. The resulting bait-target hybrids were captured with streptavidin-coated magnetic beads, removing off-target DNA. Libraries were then on an Illumina NovaSeq X Plus, generating 150bp paired-end reads across the capture region.

Raw paired-end reads were processed using the core snpArcher v1.0 workflow.[49] Briefly, the raw reads were trimmed of adapter sequences using *fastp*[50] and aligned to the *Anolis carolinensis* reference genome (rAnoCar3.1.pri, GCA_035594765.1) using *bwa-mem*.[51] We called variants using GATK,[52] using snpArcher's default settings. Variants were also filtered with snpArcher using default filtering settings. This resulting VCF file was manually filtered using *vcftools*[53] v0.1.17 to retain variants with a minimum depth of 8x coverage, a minor allele frequency that was greater than 0.05, and that contained no more than 75% missing data. These filtering statistics were chosen because they recapitulate the patterns of population divergence observed in the RADseq data the best out of several manually selected filtering schemes. This filtering reduced our snpArcher-generated VCF from 104,967 SNPs to 10,299 SNPs after filtering.

### Targeted mutagenesis of *hs6st1*

CRISPR-based gene-editing was performed on wild-caught *A. sagrei* females collected from Orlando, FL. All gene-editing experiments followed the National Research Council's Guide for the Care and Use of Laboratory Animals and were performed with the approval and oversight of the University of Georgia Institutional Animal Care and Use Committee (A2022 06-034-Y3-A9). *Anolis* gene-editing was carried out as previously reported.[42] In brief, potential Cas9 gRNA target sites in *hs6st1* were identified by retrieving *hs6st1* exon 1 sequence from the AnoSag2.1 genome reference and were chosen using CRISPOR 4.4,[54,62] selecting targets with CFD specificity scores of 95% or greater. Two *hs6st1* gRNA targets sites were selected: 5'-GGCGCACGTTCTGGACCAGG-3' and 5'-TCGAGGTGCCCTGCGACTGC-3' (Figure S2A). 10 μM *hs6st1* Cas9 RNP was produced by mixing SpCas9 2NLS with a 1:1 mixture of the two *hs6st1* sgRNAs (Synthego Corp, Menlo Park, CA) in 10 mM Tris-HCl, pH 7.4. Prior to gene editing surgeries, the ability of the *hs6st1* Cas9 RNP to cut *hs6st1* exon 1 was tested by mixing the Cas9 RNP with an *hs6st1* PCR product than spans the target site (PCR primers: *hs6st1*-F1 5'-ACCCGCACTACGTCAAGAAG-3' and *hs6st1*-R1 5'-CACGCAGTTGGTGAGCTCG-3'); the presence of DNA cleavage products was then confirmed by agarose gel electrophoresis. Oocytes of 55 adult females were injected with *hs6st1* Cas9 RNP, and the resulting eggs were collected and incubated at 29°C. After 25 days of incubation, eggs were opened, and late-stage embryos were isolated and fixed for 48 hrs in 10% buffered formalin. Embryos were screened for mutations by isolating genomic DNA from tail clips and performing Sanger sequencing of hs6st1 PCR amplicons. Geneious Prime[57] was used to visualize chromatograms for each individual, while DECODR[55] was used to analyze mutations, though high mosaicism in two individuals precluded reliable deconvolution. Sanger sequencing revealed open reading frame disrupting mutations in 5 of 55 embryos (Figure S2B). Due to the presence of complex, mosaic genotypes, additional Oxford Nanopore sequencing was conducted on two mutants. Nanopore reads were analyzed using CRISPRLungo[56] and results were verified manually with Geneious Prime. No evidence of wild-type alleles was detected in four of the five mutants, while one individual (hs6st1-AI 11) displayed 6.85% wild-type alleles in the first exon of *hs6st1*.

External morphology was measured for hs6st1 knockout (N = 5) and wild-type anoles (N = 50) from dorsal images captured using an Olympus SZX7 stereoscope and an Imaging Source DFK 37BUX250 microscope camera. On each image, snout–vent length (SVL) was measured from the tip of the snout to immediately posterior to the hindlimbs. Femur length was measured from the hindlimb insertion to the femorotibial joint. Tibia length was measured from the femorotibial joint to the talocrural joint. Metatarsus length was measured from the proximal end of the metatarsus to the base of the fourth toe of the hindfoot. Toe length was measured from the base of the fourth toe to the toe tip, excluding the claw. Measurements were extracted using Fiji V2.14[58] and each measurement was taken three times, and the average was used for downstream analyses. For bilateral phenotypes, the left and right sides were measured separately and retained for further analysis. Limb measurements were $\log_{10}$-transformed prior to analyses.

After taking measurements from whole specimens, left and right hindlimbs were removed using dissection scissors (Fine Science Tools). Skin was removed from each limb using Dumont #5 forceps. Cartilage and mineralized bone was stained and remaining tissue was cleared following the protocol of Griffing et al.[63] Briefly, cartilage was stained with Alcian Blue 8 GX, excess tissue is digested using a 1% trypsin solution, mineralized bone was stained with Alizarin Red S, and tissue was cleared using 0.5% potassium hydroxide (KOH) and glycerol.[64,65] We visualized and photographed all specimens using an Olympus SZX7 stereoscope and an Imaging Source DFK 37BUX250 microscope camera.

All individuals displayed low levels of overall bone ossification throughout their skeleton. For this reason, we did not include any measurements of ossified bone in our final analyses for concerns of measurement accuracy. For each individual, bone length and cartilage area were measured for the tibia, fibula, metatarsal, first phalanx of the fourth hind toe, and second phalanx of the fourth

hind toe. The length of each long bone was measured from the distal to proximal ends, while cartilage area was measured by identifying and extracting the region where Alcian Blue 8 GX staining was visibly present. Cartilage in the distal and proximal epiphyses were summed to calculate a total cartilage area per bone. Each measurement was taken three times for each bone using Fiji V2.4[58] and averaged. Because the left and right sides were retained, we included individual as a random effect in our linear mixed effect models to account for the non-independence of repeated measurements.

### High wind clinging experiment and analyses

We collected 62 adult male *Anolis sagrei* from Miami, Florida from August 7$^{th}$ – 10$^{th}$, 2023 and transported them back Princeton University. The lizards were singly housed and fed crickets and mealworms three times a week, while water was provided *ad libitum*. Clinging ability of each lizard under tropical storm wind speeds was estimated using a custom-fabricated Windshaper (testing section: 30cm x 30 cm, Tyoto Robotics, Gatineau, QC, Canada) to generate tropical storm wind speeds approximating the upper limit of tropical storm classification (63 - 118 km/h) under controlled laboratory conditions. Lizards were placed on a 1.27 cm diameter wooden dowel 40cm from the wind source with their head oriented upward. Wind speed was steadily increased over a 10 second interval to reach the maximum wind speeds possible. This gave the animal enough time to hold on to the perch while reducing the chance of it jumping off the perch and escaping before testing. We tested performance three times in succession and retained all trials for further analysis. Performance experiments were conducted from October 17$^{th}$ – October 20$^{th}$, 2023. Each trial was recorded at 120 frames per second using a Sony DSC-RX100M6 digital camera. All experimental procedures were approved by Princeton IACUC (3119).

We took x-ray images from all individuals in the study to identify morphological correlates to performance. Third metacarpal, radius, ulna, humerus, femur, tibia, fibula, fourth metatarsal, first and second phalanx lengths of the fourth rear toe, and pectoral girdle width, pelvic girdle width, and snout-vent length were obtained from the X-ray images. Measurements were taken using Fiji V2.4.[58] Each measure was taken three times and averaged. Left and right sides were averaged for further analyses, while right side measurements were retained for specific lines of investigation. All limb bones were standardized to body size by creating $\log_{10}$ – $\log_{10}$ regressions of each measure to SVL. Residuals were used for downstream analyses.

## QUANTIFICATION AND STATISTICAL ANALYSIS

### Analyses of genomic data

To quantify patterns of hurricane-induced migration between islands before and/or after the focal hurricane season, we conducted a discriminant analysis of principal components with the *adegenet* package[59] in R.[66] To identify the number of clusters best fit to the data, we first used the find.clusters() function to estimate the cumulative variance explained as a function of the number of principal components retained in the analysis. No discernable plateau in cumulative variance was observed across the first 150 PCs (Figure S1B, so all were retained for downstream analyses. Bayesian information criterion was then used to assess the fit of each of 40 models (number of clusters: 1-40) and the model with the lowest BIC value (number of clusters = 2) was used as the best fit model for the data (Figure S1A). To test for evidence of demographic impacts on the island populations resulting from the extreme hurricane season. Surprisingly, we detected no significant signal of demographic impact on either population. Post-storm populations did not display a significant excess of rare genetic variants (estimated by Tajima's D) as expected from a population bottleneck event (multiple linear model; Year: Pr >|t| = 0.7389; Site: Pr >|t| = 0.0831; Site*Year: Pr >|t| = 0.0829), suggesting that lizard mortality was not significant enough to result in a severe population decline (Figure S1C).

To identify regions of the *Anolis scriptus* genome displaying parallel signatures of selection across Pine Cay and Water Cay, we utilized the population branch statistic[21] to quantify polarized genomic divergence for the surviving populations on each island. We selected autosomal genotypes in PLINK[60] (v1.90b.3.45) and utilized VCFtools[53] (v0.1.14) to select genotypes with Depth (DP) > 8, genotype quality (GQ) > 20), biallelic SNPs with <20% missing data. To test for signatures of selection specific to post-hurricane survivors, calculated the population branch statistic (PBS) at single SNP resolution following Yi et al.[21] Briefly, we calculated Weir and Cocheran's $_{FST}$ between all population pairs using VCFtools.[53] We then performed a Cavalli-Sforza transformation of $F_{ST}$ values.[21] Transformed values were then used to calculate the three branch PBS[21] for each island using the surviving population as the focal group, the pre-storm population on the same island as the sister group and the pre-storm population from the alternative island as the outgroup. We then set negative values to 0, z-score normalized PBS values and calculated cumulative distribution functions to calculate p-value with *pnorm* function in R. Threshold cutoff of zscore > 4 was utilized in identifying outlier SNPs, representing genomic regions displaying elevated differentiation specific to the surviving populations on each island. We identified a total of 1622 outlier SNPs between the two islands. Of those, 1158 SNPs are present on both islands. 74 of those SNPs were shared outliers between the two islands, 36 of which overlap genes. Those 36 SNPs overlap 5 genes: cntn3 (2 SNPs), hs6st1 (20 SNPs), pdzrn3 (3 SNPs), ppp4r2 (8 SNPs), and tnpo1 (3 SNPs) (see Table S1).

Additionally, to account for drift beyond the standard 3-branch PBS, we utilized the related statistical approaches of population branch excess (PBE),[67] which further accounts for genome-wide drift by rescaling branch lengths with respect to all loci in the genome, and normalized population branch statistic (PBSn1),[68] which rescales the branch lengths of the focal population with respect to the outgroup branch lengths. Simulation studies have shown that, under some demographic scenarios, PBE and PBSn1 can outperform PBS at detecting site-specific selection.[69] We have found that the three statistics are highly correlated with each other on both islands (Figures S1D and S1E). Therefore, we searched for genomic regions that overlapped at the upper

Please cite this article in press as: Vaughn et al., Genomic targets of hurricane-induced selection on clinging performance in an island lizard, Current Biology (2026), https://doi.org/10.1016/j.cub.2026.07.022



1% of the empirical distributions for at least two of the three statistics (PBS, PBE, PBSn1; See Table S2). Only regions supported by both the zPBS outlier analysis and the cross-statistic comparison were taken as the strongest candidates for hurricane-induced parallel selection.

To calculated associations between candidate regions and each phenotype that shifted in in parallel across both islands after the hurricane season, we conducted genotype association tests using a logistic linear mixed effects model (binomial family) implemented with the functions *fitNullModel* and *assocTestSingle* in the R package GENESIS,[31] using a 500bp windows. To account for demographic structure across islands, we incorporated a genetic relatedness matrix and island as covariates. We identified outlier SNPs as the smallest 1% of the distribution of *P*-values for the association test and identified outlier genes as those containing at least one outlier SNP. From each analysis we extracted the chromosomal region associated with our *a priori* defined candidate regions to identify SNPs therein displaying significant associations each phenotype ($p < 0.05$).

## Integration of selection and trait association

To identify variants associated with both adaptive divergence and trait variation, we integrated evidence from Pine Cay PBE tests, Water Cay PBE tests and genome-wide association tests (GWAS) for the length of the longest rear toe. For each SNP, the three P-values were combined using the harmonic mean P-value (HMP) method, which is robust to heterogeneous evidence across multiple tests and reduces the influence of a single extreme P-value. The combined probability for each SNP was calculated as:

$$p_{combined} = \frac{k}{\sum_{i=1}^{k} \frac{1}{p_i}},$$

where $k$is the number of statistical tests combined and $p_i$are the individual P-values from the PBE and GWAS analyses. A SNP-level combined score was then defined as:

$$\text{combined score} = -\log_{10}(p_{combined}).$$

To quantify the consistency of evidence across statistical tests, we calculated a support metric representing the proportion of tests for which the SNP showed significant association.

For each SNP:

$$\text{support} = \frac{\text{number of tests with } p < 0.01}{\text{number of tests evaluated}}.$$

A SNP-level **local score** was then defined as

$$\text{local score} = (-\log_{10}(p_{combined})) \times \text{support}.$$

This metric prioritizes SNPs showing both strong statistical support and consistent evidence across multiple analyses. Gene annotations were obtained from the *A. carolinensis* genome annotation (rAnoCar3.1) and SNPs were assigned to genes if their genomic position fell between the annotated gene start and end coordinates. For each gene, all SNPs located within the gene interval were identified and used to calculate gene-level summary statistics.

Gene-level evidence for trait-associated selection was summarized using the SNP-level local scores of all variants within each gene. For each gene we calculated the number of SNPs located within the gene the number of supported SNPs (SNPs with support $\geq$ 2/3) and the mean of the three highest SNP-level local scores The primary gene-level statistic was defined as

$$\text{gene score} = \text{mean of top 3 SNP local scores} \times \log_{10}(n_{supportedSNPs} + 1).$$

This approach emphasizes genes containing multiple SNPs with strong and consistent statistical support while reducing the influence of isolated outlier variants. The raw gene score statistic for each gene was then scaled by the gene length:

$$S_{\text{gene}}^{(\text{length-scaled})} = \frac{S_{\text{raw},g}}{\log_{10}(L_g + c)},$$

where $c = 10$is a small offset to stabilize scaling.

Each scoring method was applied separately to PBS-only signal (parallelism), GWAS-only signal (association) and Total integrated signal (co-localization of parallelism and association). Genes were then ranked according to their gene scores in each category (See Table S3). Candidate genes were defined as those displaying consistent high rankings (top 5) across all three statistics. Within candidate genes, supporting SNPs (as defined above) were further evaluated based on their genomic location relative to gene features to assess potential functional relevance.

## hs6st1 CRISPR knockout symmetry analysis

To assess whether the hs6st1 genotype influenced bilateral symmetry in our phenotypes, we quantified asymmetry for each trait as the difference between the right and left values (right side - left side). Modeling each asymmetry index using linear mixed models, we found that the KO genotype had a greater degree of asymmetry for the second phalanx of the fourth hind toe ($p = 0.002$) compared to

wild-type individuals. Interestingly, wild-types displayed greater degrees of asymmetry of the metatarsal cartilage area ($p = 0.036$) compared to the KO genotype. To determine whether the genotype effect on second phalanx length was consistent across both sides of the animal, we reran the linear mixed effect model on the left and right sides independently. We found that the genotype effect was driven primarily by the left side, where wild-type individuals had significantly longer second phalanges than KO individuals ($p = 0.002$), while the right side showed no significant genotype effect ($p = 0.16$), indicating that the two sides contribute unequally to the overall genotype difference observed in the repeated measures analysis.

### High wind clinging analyses

Each performance trial was digitized using DeepLabCut.[43] Two models were created, one to track the lizard, and one to extract the position of the perch. The lizard tracking model was trained using 588 frames from 66 videos. The model was trained to track the position of the snout, eye, hand, elbow, shoulder, hip, knee, foot, fourth toe, tail base, and tail tip. Due to camera positioning, we only digitized the right side of each animal. Upon annotation of the training dataset, the model was trained through 100,000 iterations. To obtain the position of the perch, a model was trained using 117 frames from 6 videos through 50,000 iterations. This model was trained to extract the top and bottom of the perch. These models were used to extract lizard and perch position data from every frame of 189 videos. For each video, x and y coordinates and a likelihood score were generated for each tracked point and used for further analyses (supplemental information). For the lizard tracking model, a filtered csv file was used for further analysis, which applies a tracking probability cutoff to enhance model performance.[43]

All subsequent analyses were conducted in R.[66] We set a new coordinate system with origins along the perch axis to calculate the exact frame in which the lizard lost its grip on the perch. The positions of the top and bottom of the perch in each video were extracted and used for further analysis. Release times of the right forelimb and hindlimb were calculated based on when the forefoot or hindfoot passed the threshold of the perch. Each video was manually trimmed to begin at trial onset and end when the lizard exits the frame. The full release time, when the lizard falls completely off the perch, was calculated by removing 10 frames from each video, reflecting the time it took for lizards to exit the frame after releasing from the perch. Release time was calculated in seconds and used as the metric for clinging success. Elbow and knee angles were also calculated by defining a vector from the proximal to the distal position of each limb segment. We calculated the change in elbow and knee angles from the start of the trial to forelimb or hindlimb release, respectively. This was done by taking the mean joint angle across 10 frames for the start of the trial and subtracting it from the mean of 10 frames right before limb release. We used these measures for downstream analyses.

To investigate the relative contribution of skeletal morphology and positioning to overall clinging performance under high wind speed conditions, we used linear mixed effects models. We first built a full model consisting of the change in elbow and knee angles, size-standardized limb bone lengths, and all biologically relevant interactions to predict full release time. All variables (change in elbow and knee angles, size-standardized limb bone lengths, and full release time) were scaled to have a mean of 0 and 1 standard deviation before being incorporated into the model. Additional models were built whereby we iteratively removed fixed effects and compared it to the full model using likelihood ratio tests. All models contained random effects of individual and trial to account for the effects of successive performance measurements.

Our analyses revealed that, in the high wind speed trials, the forelimbs of the anoles were able to maintain their grip on the perch significantly longer than the hindlimbs (See main text for statistical details). To understand how variation in limb-specific clinging duration impacts overall release time, we fit a mixed linear model consisting of forelimb clinging duration, hindlimb clinging duration, and their interaction to overall clinging duration. All clinging durations were scaled to mean 0 and 1 standard deviation before being incorporated into the model. This model, along with all models described below, contained random effects of ID and Trial to account for the effects of successive measures from the same individual. We found that forelimb clinging time positively affects overall clinging ability (Estimate: 0.777, df = 179.05, $p < 0.0001$; Figure S3F), with neither the hindlimb or the interaction playing a significant role ($p > 0.05$). However, hindlimb release time was also a significant predictor of forelimb release time (Estimate: 0.773, df = 178.39, $p < 0.0001$; Figure S3G), suggesting that early hindlimb release imposes greater stress on the forelimbs during extended clinging. This is likely due to the two-fold stress of reduced surface area making direct contact with the substrate and the increase in supported mass added by the unattached hindlimbs. Therefore, favorable variation would be such that it increases hindlimb clinging duration, thereby improving forelimb clinging ability, and ultimately contributing to greater overall clinging performance.

To assess the importance of body morphology and kinematics on forelimb clinging duration, we fit another linear mixed model to all size-standardized forelimb bone residuals (third metacarpal, radius, ulna, and humerus lengths), kinematics (change in elbow angle during the trial), and biologically-relevant interactions to forelimb clinging duration. Due to the camera position, we could only track the right side of the animal, so we only used the right morphological traits to fit this model. All variables (limb bone residuals, forelimb kinematics, and forelimb clinging duration) were scaled to mean 0 and standard deviation 1 before incorporation into the model.

We found that the change in elbow angle was a significant positive contributor to forelimb clinging time (Estimate: 2.17, df = 151.87, $p = 0.023$). Forelimb kinematics were also at the center of further higher order interactions with forelimb morphology, including interactions between the change in elbow angle and radius length (Estimate: -0.371, df = 154.85, $p = 0.0301$), change in elbow angle, ulna, and radius length (Estimate: -0.167, df = 145.68, $p = 0.041$), and change in elbow angle, humerus, ulna, and radius length (Estimate: 0.155, df = 140.21, $p = 0.0448$). Taken together, it seems that both the variation in forelimb kinematics and the relative ratios of the forelimb skeletal elements drive forelimb clinging time variation.

Analyses of the determinants of hindlimb clinging performance reveal that both kinematic (change in knee angle during the trial) and morphological variables influence hindlimb clinging ability. Hindlimb kinematics was a significant negative contributor to hindlimb

Please cite this article in press as: Vaughn et al., Genomic targets of hurricane-induced selection on clinging performance in an island lizard, Current Biology (2026), https://doi.org/10.1016/j.cub.2026.07.022



clinging time (Estimate: -0.214, df = 155.98, p = 0.0105), while the length of the first phalanx contributes positively (Estimate: 0.287, df = 153.98, p =0.0087). Significant interaction effects between morphological variables also shape hindlimb clinging ability, including a negative interactive effect of the first and second phalanges (Estimate: -0.184, df = 154.34, p = 0.039), and a positive interactive effect of tibia and fibula lengths (Estimate: 0.313, df = 154.0, p = 0.009).

To identify the morphological correlates to forelimb kinematics, we fit a linear mixed model containing all scaled, size-standardized forelimb bone residuals to the change in elbow angle during the trial. We found that the metacarpal length contributes positively to the change in elbow angle during high wind speed conditions (Estimate: 0.158, df = 169.0, p = 0.043). Fitting a linear mixed model as described above, we found that the tibia is also a positive contributor to the change in knee angle during hurricane conditions (Estimate: 0.201, df = 55.28, p = 0.024).

In summary, our results demonstrate that overall clinging ability in high wind conditions is primarily driven by forelimb performance, which itself is influenced by forelimb kinematics and morphology. While forelimb clinging time has the strongest direct effect on overall performance, hindlimb clinging time indirectly contributes by potentially influencing forelimb strain. We also show that skeletal traits contribute to limb kinematic variation during high wind speed conditions. Taken together, these results suggest that an integrated suite of morphological and kinematic traits acting both at the limb level and across the whole organism form the basis for performance under extreme environmental stress.

### Comparison of *A. sagrei* and *A. scriptus*

To ensure that species-specific differences in fourth toe morphology between *Anolis scriptus* and *A. sagrei* didn't bias the results of our high wind speed performance experiments, we evaluated the extent of morphological overlap between the two species. First, we calculated residual fourth toe length by creating log10 - log10 regressions against body size (SVL), combining both species into the same model. This approach allowed us to compare relative toe lengths across species independent of body size. We then examined the distribution of residual toe lengths across our two species (Figure S3H). We identified 7 *A. sagrei* individuals that fell outside of the range of the pre-storm *A. scriptus* populations, representing ~11% of our total *A. sagrei* sample size, with 6 individuals having residual fourth toe lengths greater than this range and a single individual possessing a smaller relative trait value. Because these individuals represent morphology not present in our *A. scriptus* sample at the time of selection, we conducted an analysis to test if the exclusion of those individuals altered the functional relationship between toe morphology and clinging performance. We repeated the linear mixed model analysis relating fourth toe length to clinging performance in *A. sagrei* on the data set that only contained individuals that had overlapping fourth toe residuals with the *A. scriptus*. When doing so, we found that the first phalanx of the fourth hind toe still remains significant, with the estimate remaining consistent with the inclusive model (Overlapping Model: N = 56, Estimate = -0.545, df = 28.1, p = 0.045; Full Model: N = 63, Estimate = -0.573, df = 30.1, p = 0.042; See main text for statistical details regarding the linear mixed effects models). Together, these results indicate that our functional analysis is robust to the exclusion of individuals that lie beyond the variation present at the time of selection.